Universal correlations after thermalization in periodic nonlinear systems

IOP Publishing Journal of Physics B: Atomic, Molecular and Optical Physics
J. Phys. B: At. Mol. Opt. Phys. **51** (2018) 035401 (14pp) https://doi.org/10.1088/1361-6455/aa9a97

Universal correlations after thermalization in periodic nonlinear systems

Uri Levy[1], **Ken Yang**[2], **Noam Matzliah**[1] **and Yaron Silberberg**[1]

[1] Weizmann Institute of Science, Rehovot 7610001, Israel
[2] State Key Laboratory of Optoelectronic Materials and Technologies, Sun Yat-sen University, Guangzhou 510275, People's Republic of China

E-mail: uri.levy@weizmann.ac.il

Received 16 August 2017, revised 22 October 2017
Accepted for publication 14 November 2017
Published 8 January 2018

Abstract

The evolution of random fields with known statistical properties is relatively straightforward to analyze in the linear regime, but becomes considerably more involved when nonlinearity, or interactions, are dominant. Previous works have shown that statistical physics techniques can be applied to predict the evolution of such systems. Here we study the evolution of random fields in a one-dimensional lattice of optical waveguides in the presence of strong nonlinearities, using the discrete nonlinear Schrödinger equation. Extending the 2009 work by Silberberg *et al* (*Phys. Rev. Lett.* **102** 233904), we assume input fields with random amplitudes and phases. We derive analytic expressions for the system's statistical properties at thermodynamic equilibrium. Specifically, expressions for the probability density functions of field intensities, of fields' phase differences, and an expression for the field correlations. We express these properties in terms of the moments of the assumed statistical excitations, and verify the results with simulations. Most interestingly, we find that at thermodynamic equilibrium, correlations are formed through the interaction between sites. These exponentially decaying fields' correlations take a universal form that is essentially independent of excitation amplitudes but visibly shrink with increased spread of the exciting amplitudes. Our results are valid not only to nonlinear discrete optical systems, but extend also to the evolution of bosonic atoms in optical lattices in the high-occupancy limit that are governed by the equivalent Gross–Pitaevskii equation.

Keywords: nonlinear optics, optical waveguides, optical lattices, Kerr nonlinearity, correlation functions, periodic structures, Bose–Einstein condensates

(Some figures may appear in colour only in the online journal)

1. Introduction

A key characteristic of evolving discrete nonlinear systems with interacting neighboring sites is the formation of field correlations. That is—as these systems evolve following certain random excitations, the site-fields, through site-allowed interactions, influence each other such that correlations are formed [1]. Discrete systems can be very small starting from only two sites of a bosonic Josephson junction [2], or of two and three sites dimers and trimers [3–5]. Or can be very large such as long one dimensional [6] or few dimensional [7] polymer chains, or continuous systems of discrete particles [8]. And in the analysis of these and other discrete systems, correlations play an important role [9]. Field correlations relate to observable quantities [10]. As an example, an abrupt change in the radial correlation curve (from algebraic decay to exponential decay through an increased temperature step) signifies a Berezinskii–Kosterlitz–Thouless phase transition. This was demonstrated experimentally by Hadzibabic *et al* using a 2D cloud of ^{87}Rb atoms [11] and shown analytically and numerically by Small *et al* for a 2D lattice of optical waveguides [12]. As another example in the context of zero temperature bosonic atoms in a double-well trap, Galante *et al* expressed coherence visibility in terms of correlation of consecutive expansion coefficients of a zero temperature energy state in a Fock basis (with a different version of defined correlation compared to the fields' correlation version defined below [13]).

The most frequently used equation prescribing the evolution dynamics of discrete nonlinear systems is the discrete nonlinear Schrödinger equation (DNLSE) [14–16]. Systems of various nature—ultracold atoms trapped in optical lattices, coupled mechanical oscillators, polarons in ionic crystals, light through discrete optical waveguides, evolve according to the DNLSE. Several papers and books review the properties of the DNLSE [15, 17–19].

In their 2009 paper, Silberberg *et al* discussed universal correlations formed in a 1D lattice of periodic optical waveguides under DNLSE dynamics [1]. Assuming excitation of all waveguides by constant amplitudes and uniformly-distributed random phases, the authors of [1] calculated exponentially decaying correlations (of the fields). In our work reported here we extend the analysis of [1] to finite-width Gaussian excitations (with the excitation conditions assumed in [1] as the limiting case of zero Gaussian width). This is a natural extension to more general cases where the exciting amplitudes are not strictly uniform. We find, interestingly, that for any non-zero spread of excitation amplitudes, although the formed correlations are weaker and shorter (versus those for no spread), universality is still preserved. Namely, formed field correlations are independent of amplitudes' average value.

Studies of coupled nonlinear optical waveguides have already been published in quite a few papers in the last 30 years ([20–26] to cite a few). But unlike most of those studies where initial waveguide excitation conditions placed the studied systems in the breather-forming regime of the phase diagram, we treat systems on or slightly above the strong-interaction line in the no-breathers region [27] (see figure 2 below). We derive probability density functions for the site intensities and for neighboring sites phase differences and calculate field correlations. As in [1], we find exponentially decaying field correlations. We further show that correlations decay faster as the spread of the Gaussian excitation grows. Surly, our results apply to the mentioned other physical systems that evolve under DNLSE dynamics.

The evolution of light propagation through periodic optical waveguides is similar, under certain conditions, to the evolution of ultracold atoms in periodic traps (see a BEC review [28] and for a study of system relaxation from non-equilibrium states [29]). A brief discussion of the conditions for similarity follows.

The Hamiltonian underlying the DNLSE (equation (1) below) consists of two terms: a linear ('kinetic energy') term and a cubic ('interaction') term: $\mathcal{H} = \sum_{m=1}^{N} [U_m(z)U_{m+1}^*(z) + U_m^*(z)U_{m+1}(z)] + \frac{\Gamma}{2}\sum_{m=1}^{N}|U_m(z)|^4$ where $U_m(z)$ is a dimensional complex field at site m at distance z, and $|U_m(z)|^2$ is the site's intensity at distance z. A classical version of free space (no external potential) Gross–Pitaevskii (GP) Hamiltonian for ultracold bosonic atoms occupying an optical lattice with high numbers in each trap is actually identical: $\mathcal{H}_{\mathrm{GP}} = \sum_{m=1}^{N}[\psi_m(t)\psi_{m+1}^*(t) + \psi_m^*(t)\psi_{m+1}(t)] + \frac{\mathrm{U}}{2J}\sum_{m=1}^{N}|\psi_m(t)|^4$ [30–32]. Here $\psi_m(t)$ is dimensional (unlike in [31]), representing the matter wave at site m at time t. Now, whereas the DNLSE dynamics for the optical system holds for any value of $U_m(z)$, i.e. the interaction term can be (theoretically) arbitrarily strong (and there is no BEC-characteristic excitation gap [33]), the GP dynamics holds only up to a certain interaction strength. Beyond this interaction strength the cold bosonic atoms go through a quantum phase transition (from a superfluid to a Mott insulator) [34], and the dynamics can no longer be described by the GP equation [35].

Here, for the initialization of the optical system we *have* assumed strong interactions. In terms of cold bosonic atoms then, our analysis applies to a quench study [36, 37]. First the system is prepared in a Mott configuration—high and almost uniform occupation numbers [38] and completely random phases. Or, to describe it from a different angle, the system is prepared in a highly number squeezed state [39, 40]. Then, at time $t = 0$ the system's parameters are abruptly changed (for example by reducing the optical barriers) such that the system evolves to a new equilibrium under GP dynamics [29, 31]. Under such quench situations our results for optical systems hold for the atomic system as well.

2. Equation of motion and conserved quantities

The fields' evolution dynamics considered here is described by a 1D periodic 'cubic' [41] DNLSE in its simplest version [17]: $\mathrm{i}\frac{\mathrm{d}U_m(\zeta)}{\mathrm{d}\zeta} = -C[U_{m-1}(\zeta) + U_{m+1}(\zeta)] - \gamma\,|U_m(\zeta)|^2 U_m(\zeta)$. Here U_m is the field at site m at position ζ, C and γ are the coupling coefficient to nearest neighbors and the (material in the case of waveguides) nonlinearity coefficient respectively. Born–von Karman [42] (cyclic) boundary conditions are assumed. After dividing by the coupling coefficient the equation reads:

$$\mathrm{i}\frac{\mathrm{d}U_m(z)}{\mathrm{d}z} = -[U_{m-1}(z) + U_{m+1}(z)] - \Gamma\,|U_m(z)|^2 U_m(z)$$
$$z = C\zeta; \qquad \Gamma \equiv \gamma/C. \tag{1}$$

The evolution coordinate (z) is now dimensionless and the nonlinearity coefficient (Γ) has the dimensions of $|U_m(z)|^{-2}$. Throughout this paper, as in [43], we keep the value of the nonlinearity coefficient at $|\Gamma| = 1$. The nonlinearity of site m at point z is thus determined by the amplitude (squared) of the site field—$\mathrm{sign}(\Gamma)\ |U_m(z)|^2$.

Let us briefly pause here to look at the linear plus nonlinear two-term evolution equation (1).

From the point of view of the optics community, the linear term is a nearest neighbors energy coupling term, where the details of the fields between the (widely-separated) waveguides, both in the single-level tight binding model or according to the coupled-mode theory (CMT), are packed into the coupling coefficient [44, 45]. Actually, the origin of optical-energy coupling is material polarization: neighboring-fields are radiated (90° out of phase) by the field-excited material polarization [46, 47]. The end result is of course

energy tunneling, much like energy tunneling of matter waves through potential barriers [48]. From the point of view of the BEC community, the linear 'kinetic energy' term is just the discrete version of the Laplacian operator [49]. (The missing $-2U_m(z)$ 'diagonal' term in equation (1) [49] can be restored by a simple global transformation [50] so that the two versions of the equation—with and without the $-2U_m(z)$ term—are equivalent).

The second, Kerr-like nonlinear term, is a particle–particle, on-site interaction term. With very different origin comparing mass-less photons to massive particles. Photon–photon interaction is again mediated by material polarization. As a result, given the material selected, control of the nonlinearity coefficient can be achieved through material-induced changes, which are hard to implement. But the optical nonlinearity strength can be high, limited only by material damage threshold. Ultracold bosonic atoms directly attract-repel each other. The interaction strength is lumped into an s-wave scattering length [30]. This pair-interaction strength can be controlled [51] and even sign inverted [52] by an external magnetic field. Yet the density (and hence nonlinearity strength) of site-trapped atoms is limited through three-body recombinations [39, 53], and through other effects.

Energy bands are normally associated with periodic structures [44], also in the cases where nonlinearity is included [45, 54]. For a 1D Kronig–Penney lattice (periodic square wells) analytic solutions are known [55, 56], and yield structure and stability properties similar to the properties under sinusoidal potentials (as in BEC experiments) [56]. However, energy bands are *not* generated by the CMT-like DNLSE (equation (1)), and we straightforwardly solve the equation numerically, applying the Runge–Kutta method.

A final note for the properties of equation (1), related to focusing–defocusing. Writing the equation as $\mathrm{i}\frac{\mathrm{d}U_m(\zeta)}{\mathrm{d}\zeta} = -C[U_{m-1}(\zeta) + U_{m+1}(\zeta)] - \gamma|U_m(\zeta)|^2U_m(\zeta)$, positive (negative) nonlinearity coefficient (γ) is 'focusing' ('defocusing') [1]. In terms of ultra-cold atoms, 'attractive' ('repulsive') is focusing (defocusing) [57]. More generally, if the two real coefficients ($-C$, $-\gamma$) on the right hand side of the DNLSE are of the same (opposite) sign, then the system is referred to as 'focusing' ('defocusing') [32]. In optics, negative nonlinearity (γ) is rare so systems are usually focusing, whereas in BECs repulsive interactions, yielding defocusing systems (that may lead to dark solitons [58]), are typical [28, 30].

Back to equation (1) now, it is convenient to write the complex field U_m as a product of amplitude u_m (a real non-negative number) and a phase factor—$\exp(\mathrm{i}\cdot\phi_m)$:

$$U_m \equiv u_m \mathrm{e}^{\mathrm{i}\phi_m};\ \ I_m \equiv U_m U_m^* = u_m^2. \tag{2}$$

Correlations of (any) two fields at 'distance' k of each other ($C_k(z)$) are defined as the average $C_k(z) = \frac{1}{2N}\sum_1^N[U_m^*(z)U_{m+k}(z) + U_m(z)U_{m+k}^*(z)]$ where N is the total number of sites. Or, using equation (2):

$$C_k(z) = \frac{1}{N}\sum_{m=1}^{N} u_m(z)u_{m+k}(z)\cos[\theta_{m,k}(z)]$$
$$\theta_{m,k}(z) \equiv \phi_m - \phi_{m+k}. \tag{3}$$

Formation of these fields' correlations is a prime subject of our study. Note that in BEC studies, 'correlation' often refers to *density* fluctuations as reflected by the second order correlation function g_2 [59].

Now, unlike the integrable continuous NLS equation [60], the discrete NLS equation (1) is non integrable [16, 61], and has two constants of motion [41, 62, 63].

The first constant of motion is the Hamiltonian (or 'total energy'—$\mathcal{H}_a$), the sum of two un-conserved quantities:

$$\mathcal{H}_a = \mathcal{H}_2(z) + \mathcal{H}_4(z)$$
$$\mathcal{H}_2(z) = \frac{2}{N}\sum_{m=1}^{N} u_m(z)u_{m+1}(z)\cos[\theta_{m,1}(z)] = 2C_1(z)$$
$$\mathcal{H}_4(z) = \frac{\Gamma}{2}\frac{1}{N}\sum_{m=1}^{N} u_m^4(z). \tag{4}$$

Here $\mathcal{H}_2(z)$ is the 'kinetic energy', and $\mathcal{H}_4(z)$—the 'interaction energy'. The Hamiltonian defined by equation (4) (and down below appears in the phase diagrams of figure 2), is a site-averaged Hamiltonian. Note that since in our study the values of all u's are narrowly spread (around the shift value μ—see equation (6)), the Hamiltonian of equation (4) is approximately a nearest-neighbors quantum rotor Hamiltonian [64].

The second conserved quantity ($\mathcal{W}$) is the wave-action [27]:

$$\mathcal{W} = \frac{1}{N}\sum_{m=1}^{N} u_m^2(z) = C_0 \tag{5}$$

also written in its site-averaged version (and constitutes the horizontal axis of the phase diagram). The wave-action is also termed 'total power', 'total intensity', 'number of particles', 'density', or 'system norm' in different contexts.

With the evolution dynamics defined, our objective is to predict the long range (post-thermalization) system's characteristics given a predefined set of statistical excitations. In order to illustrate our derived general results, we have selected a specific type of system's statistical excitation. Namely—Gaussian excitation.

3. Gaussian excitation

As mentioned, we extend the work of [1] by studying DNLSE-governed systems, statistically excited with a finite-width non-negative Gaussian distribution. Amplitudes of the fields at $z = 0$ are Gaussian distributed with flat-distributed random phases, as in [1]. The system's excitation statistics

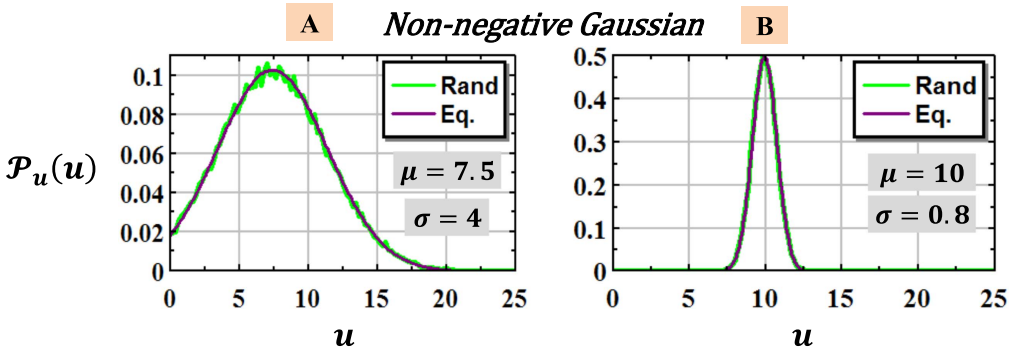

Figure 1. Non-negative Gaussians. (A) Relatively wide. (B) Relatively narrow. In all examples studied and reported below we assumed $\mu \gg \sigma$ so that for amplitudes near zero the PDF(u) is also nearly zero (i.e. only amplitudes with values close to the shift value (μ) are excited). Normal Gaussian moments could have been used. However, for the derived analytic expressions we held-on to the exact mathematics.

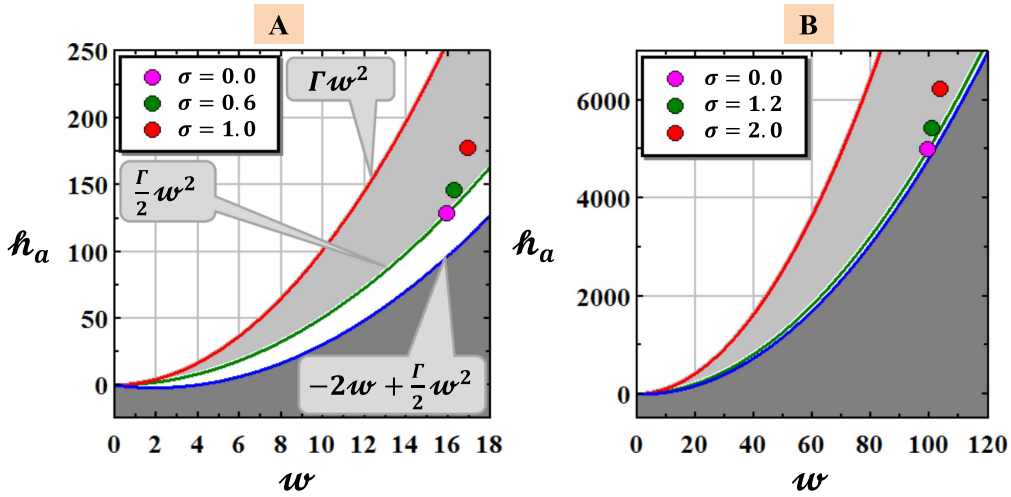

Figure 2. Position of the studied systems on the DNLSE phase diagram. The zone between the blue (zero temperature) line and the red (infinite temperature) line is the thermalization zone, further divided by the *strong-interaction* green line. The white zone above the red line is a (negative temperature) breather-forming zone, and the dark gray zone below the blue line is an inaccessible zone. (A) $\mu = 4$. (B) $\mu = 10$. As shown, with $\sigma = 0$ the systems are positioned exactly on the 'cold' strong-interaction line in the thermalization zone (the green line). With increased σ, the systems heat-up and drift upwards in the thermalization zone. The up drift is accompanied by a pronounced reduction in fields' correlation length.

takes the form:

$$\mathcal{P}_u(0 \leqslant u \leqslant \infty) = \frac{1}{\mathfrak{R}_u} \exp\left[\frac{-(u-\mu)^2}{2\sigma^2}\right]$$
$$\mathfrak{R}_u \equiv \sqrt{\frac{\pi}{2}}\sigma\left[1 + \mathrm{erf}\left(\frac{\mu}{\sqrt{2}\,\sigma}\right)\right]$$
$$\mathcal{P}_\phi(0 \leqslant \phi \leqslant 2\pi) = \frac{1}{2\pi} \Rightarrow \mathcal{P}_\theta(0 \leqslant \theta \leqslant 2\pi) = \frac{1}{2\pi}. \quad (6)$$

The non-negative Gaussian excitation (equation (6) and figure 1) varies with only two parameters—the 'shift' μ (not exactly the mean, see equation (12), and not to be confused with chemical potential), and the 'width' (or 'spread') σ.

Generally, once the statistical distribution of system's excitation is known, the expectation values (average over realizations, designated $\langle\cdot\rangle$) of the constants of motion can be calculated. Thus, the expectation value of the wave-action constant $\langle w \rangle$ is given by:

$$\langle w \rangle = \int_0^\infty u^2(0)\mathcal{P}_u(u(0))\mathrm{d}u(0) \equiv u^2(0). \quad (7)$$

The expectation value of the total energy constant $\langle \hbar_a \rangle$ is given by the sum of the (not conserved) kinetic and interaction energies ($\langle \hbar_2 \rangle$ and $\langle \hbar_4 \rangle$) at any z, including $z = 0$:

$$\langle \hbar_2(0) \rangle = 2\left[\int_0^\infty u(0)\mathcal{P}_u(u(0))\mathrm{d}u(0)\right]^2 \times \left[\int_0^\infty \cos(\theta(0))\mathcal{P}_\theta(\theta(0))\mathrm{d}\theta(0)\right] \equiv 2\,\langle u(0)\rangle^2\,\langle\cos(\theta(0))\rangle. \quad (8)$$

Equation (8) holds since the amplitudes $u(0)$'s are independent random variables. Similarly for $\langle \hbar_4 \rangle$ at $z = 0$:

$$\langle \hbar_4(0) \rangle = \frac{\Gamma}{2}\int_0^\infty u^4(0)\mathcal{P}_u(u(0))\mathrm{d}u(0) \equiv \frac{\Gamma}{2}\langle u(0)^4\rangle. \quad (9)$$

And the expectation value of the total energy constant $\langle \hbar_a \rangle$ (per site) becomes:

$$\langle \hbar_a \rangle = \langle \hbar_2(0) \rangle + \langle \hbar_4(0) \rangle. \tag{10}$$

Let us just mention that equations (7)–(10) hold for any statistical excitation (with independent random amplitudes), not just for the selected Gaussian excitation.

Given the Gaussian excitation of equation (6), the general expressions (7)–(10) can be expressed in terms of their statistical moments:

$$\begin{aligned} &\langle \omega \rangle = M_2 \\ &\hbar_2(0) = 0; \quad \langle \hbar_4(0) \rangle = \frac{\Gamma}{2} M_4 \\ &\Rightarrow \langle \hbar_a \rangle = \frac{\Gamma}{2} M_4 \end{aligned} \tag{11}$$

With (M_1 included for future use):

$$\begin{aligned} M_1 &= \mu + \frac{\sqrt{2}\,\sigma \exp\left(-\frac{\mu^2}{2\sigma^2}\right)}{\sqrt{\pi}\left[1 + \mathrm{erf}\left(\frac{\mu}{\sqrt{2}\,\sigma}\right)\right]} \\ M_2 &= \mu^2 + \sigma^2 + \frac{\sqrt{2}\,\mu\sigma \exp\left(-\frac{\mu^2}{2\sigma^2}\right)}{\sqrt{\pi}\left[1 + \mathrm{erf}\left(\frac{\mu}{\sqrt{2}\,\sigma}\right)\right]} \\ M_4 &= \mu^4 + 6\mu^2\sigma^2 + 3\sigma^4 \\ &\quad + \frac{\sqrt{2}\,\sigma(\mu^3 + 5\mu\sigma^2)\exp\left(-\frac{\mu^2}{2\sigma^2}\right)}{\sqrt{\pi}\left[1 + \mathrm{erf}\left(\frac{\mu}{\sqrt{2}\,\sigma}\right)\right]}. \end{aligned} \tag{12}$$

Note that the expressions in equation (12) are written each as the sum of a Normal (Gaussian) distribution moment and a correction term required for positive-only Gaussian distribution. It is easy then to see that for large shift μ and or small width σ (i.e. $\mu/\sigma \gg 1$), all correction terms vanish. (However, in the evaluation of the analytic equations derived below we consistently call for the exact expressions).

We now wish to relate the Gaussian-excited systems to the phase diagram.

The phase diagram associated with the DNLSE ($\hbar_a(\omega)$, see figure 2) can be grossly divided into two zones—a 'no-breathers' or thermalization zone (permits the construction of standard Gibbsian equilibrium measures for positive temperatures [43]), and a breather-forming zone ([27, 43]). The no-breathers zone is limited below by a zero temperature line ($\hbar_a = -2\omega + \frac{\Gamma}{2}\omega^2$ for $\Gamma > 0$, the blue line of figure 2), and is limited above by an infinite temperature line ($\hbar_a = \Gamma\omega^2$, the red line of figure 2). The breathers-forming zone, the zone above the infinite temperature line, is referred to as a negative temperature zone [43] and the input power to a system in the negative temperature zone must be limited from above [27]. The zone below the zero temperature line is inaccessible [43].

The no-breathers zone is further divided by a line for high nonlinearity systems ($\hbar_4(z_{ss}) \cong \hbar_a = \frac{1}{2}\Gamma\omega^2$. [27], the green line of figure 2). The green line is an approximation to the total energy under the assumption that the contribution of the linear, kinetic energy term ($=-2\omega$) is small compared to the contribution of the quadratic, interaction term $\left(\frac{1}{2}\Gamma\omega^2\right)$. In the cold atoms language—$E_{\mathrm{int}}/E_{\mathrm{kin}} \gg 1$. We refer to the green line of figure 2 as a *strong-interaction* line.

The Gaussian-excited systems discussed here are placed at or slightly above the strong-interaction line in the no-breathers zone. As can be seen from equations (11) and (12), for $\sigma = 0$, $M_4 = M_2^2$ so that the system is exactly on the $\hbar_a = \frac{1}{2}\Gamma\omega^2$ 'cold' line for all μ's. However, once σ grows above zero, the system 'heats up' and drifts upwards into the thermalization zone (figure 2). And, as we show below, this upwards drift with increased excitation width is associated with quick reduction of the fields' correlation length.

These system initializing conditions, namely—high intensity and small intensity fluctuations correspond to the conditions of an ultra-cold atoms system of high number of site particles and small number-fluctuations assumed by Danshita and Polkovnikov in their study of quantum tunneling [34].

Our objective next, given Gaussian excitation, is the derivation of analytic expressions for the probability density of site intensities $\mathcal{P}_I(I)$, and of phase differences $\mathcal{P}_\theta(\theta)$ at thermodynamic equilibrium.

4. Probability densities at thermodynamic equilibrium

For a system in the thermalization zone, the system's entropy is maximized with evolution distance [43]. We are looking then to find the long-distance PDF ($\mathcal{P}_{I,\theta}(I_1 \ldots I_N,\ \theta_1, \ldots, \theta_N)$ that maximizes system's entropy:

$$\begin{aligned} S_{I,\theta}[(\mathcal{P}_{I,\theta}(I_1 \ldots I_N,\ \theta_1, \ldots, \theta_N)] &= -\int_0^{2\pi}\int_0^{\infty} \mathcal{P}_{I,\theta} \ln(\mathcal{P}_{I,\theta}) \\ &\times \prod_1^N \mathrm{d}I_i \mathrm{d}\theta_i \end{aligned} \tag{13}$$

subject to three constraints: conserved wave-action, conserved total energy, and a normalized PDF. To find the entropy's extremum we generally need to solve the following $2N + 3$ equations:

$$\nabla_{\mathcal{P}_{I,1},\ldots,\mathcal{P}_{I,N},\mathcal{P}_{\theta,1},\ldots,\mathcal{P}_{\theta,N},\alpha,\eta,\lambda} \mathcal{L}_N(I_1 \ldots I_N,\ \theta_1, \ldots, \theta_N,\ \alpha,\ \eta,\ \lambda) = 0, \tag{14}$$

where $\mathcal{L}_N$ is the Lagrangian expression. However, following [1], since (as we show below) the intensities are not correlated, the quantum phase model [65] approximation applies. Adopting this approximation, the $I - \theta$ parameters are Gibbs-space separable variables [66] so that the PDF ($\mathcal{P}_{I,\theta}$) splits into $\mathcal{P}_I$ and $\mathcal{P}_\theta$. The system's entropy becomes the sum of intensity-entropy and phase-difference entropy ($s_{I,\theta} = s_I + s_\theta$). Thus, our task is greatly simplified. We need to solve only six

equations with four constraints:

$$\nabla_{\mathcal{P}_I,\mathcal{P}_\theta,\alpha,\eta,\lambda_1,\lambda_2}\mathcal{L}(I,\,\theta,\,\alpha,\,\eta,\,\lambda_1,\,\lambda_2)=0. \tag{15}$$

Before writing the solutions to equation (15), let us look at simulated correlations and at simulated entropy curves.

Nearest neighbors correlations are visualized by figure 3. Left column at excitation ($z=0$), right column at $z=30$. The rows, top to bottom show correlations of ϕ, θ, I. At $z=0$, Following the random excitation, no correlations are visible. Looking at (B) of the top row we clearly see fields' phase correlations formed at $z=30$. Looking at (D) of the center row, no correlations are seen, and the PDF ($\mathcal{P}_\theta(\theta)$) at $z=30$ is not flat anymore, with higher occupation near 0 and 2π radians (see figure 6). Going down to the third row, no intensity correlations are visible and the PDFs ($\mathcal{P}_I(I)$) for both E and F seem to follow Gaussian shapes (see figure 6). The no intensity correlations assumption that led to the simplified Lagrangian of equation (15) is thus verified.

Next—simulated entropy curves and simulated field correlation curves. That is—the change of entropies and correlations with evolution distance.

Entropy curves are shown in figure 4(A). The figure shows the contribution of intensity, the contribution of phase-difference (θ), and the overall (site-averaged) system's entropy ($s_{I,\theta}=s_I+s_\theta$). Interestingly, we see a weak overshoot of the intensity-contributed entropy, and a decay with small dip in the phase-difference-contributed entropy. In addition, we see very pronounced overshoots in the fields' correlation curves of figure 4(B).

Details of evolution of correlation coefficients are shown by figure 5. At short distances by figure 5(A) and at longer distances by the zoom out of figure 5(B). The figure shows three curves of evolution of the correlation coefficient, one for each of the following three variables—the phase of the fields (ϕ), the phase difference (θ), and the site-intensity ($I=u^2$). Correlation here, at every distance z, is between the array of each variable and its k-shifted version (for the simulations of figure 5 $k=1$). Correlation coefficient is defined in the standard way: if the array is x_0 and its k-shifted version is x_k then $\rho(x_0,\,x_k)=\frac{E[x_0x_k]-(E[x_0])^2}{\mathrm{VAR}[x_0]}$ (since $E[x_0]=E[x_k]$ and $\mathrm{VAR}[x_0]=\mathrm{VAR}[x_k]$). The shown curves are the average of ten realizations. Note the difference between phase correlations defined here and phase correlations defined in a recently published work by Santra *et al* [67].

At short distances, correlations are formed in all the three shown variables. However, phase-difference correlations and intensity correlations decay with further propagation and only the phase correlations persist to thermodynamic equilibrium. These phase correlations are intimately related to the fields' correlations discussed in section 5.

Back to equation (15), after accepting another approximation $\left[\exp\left(-\frac{\eta\Gamma M_2^2}{2}\right)/(\eta\Gamma)\cong 0\right]$, we find its solutions, yielding the two thought-for PDFs:

$$\begin{aligned}
&\mathcal{P}_I(I)=\frac{1}{\mathfrak{R}_I}\mathrm{e}^{-\frac{\eta\Gamma}{2}(I-M_2)^2}\\
&\mathfrak{R}_I=\sqrt{\frac{\pi}{2\eta\Gamma}}\left[1+\mathrm{erf}\left(M_2\sqrt{\frac{\eta\Gamma}{2}}\right)\right]\\
&\mathcal{P}_\theta(\theta)=\frac{1}{2\pi\mathcal{I}_0(2\eta M_1^2)}\mathrm{e}^{-[2\eta M_1^2\cos(\theta)]}\\
&\eta\left\{\left[4M_1^2\int_0^{2\pi}\cos(\theta)\mathcal{P}_\theta(\theta)\mathrm{d}\theta\right]\right.\\
&\quad\left.-|\Gamma|(M_4-M_2^2)\right\}+1=0\\
&\mathrm{sign}(\eta)=\mathrm{sign}(\Gamma)
\end{aligned} \tag{16}$$

where $\mathcal{I}_0(z)$ is the modified Bessel function of the first kind.

The Lagrange multiplier η appearing in the PDFs expressions is the solution to the implicit equation given in (16) and is of course, indirectly, a function of the shift μ and the width σ of the excitation statistics. We have found numerically that for a fixed σ, the product ηM_1^2 is constant, surprisingly independent of the shift μ so that $\eta=C_\sigma(\sigma)/M_1^2$ with $C_\sigma(\sigma)$ a monotonically decreasing function, $C_\sigma(\sigma=0)\cong 0.533$. For large μ then, indeed $\left[\exp\left(-\frac{\eta\Gamma M_2^2}{2}\right)/(\eta\Gamma)\cong 0\right]$.

Probability density functions, simulated and calculated according to the expressions of equation (16) are depicted by figure 6. Note that the expressions in equation (16) are general and are *not* specific to Gaussian excitation. They hold for random flat-distributed phase excitation and high nonlinearity (practically, in our examples studied here, $\mu>3$ and $\sigma\ll\mu$ yield reasonable fits).

With PDFs expressions in place, we can move on to discussing field correlations.

5. Field correlations

Field correlations are defined by equation (3). Since the intensities (and therefore $u_m(z)$) were shown to be uncorrelated, the expectation $\langle C_k\rangle$ of the fields' correlation, i.e. the average over realizations, is given by

$$\langle C_k\rangle=\langle\sqrt{I}\rangle^2\langle\cos(\theta_k)\rangle \tag{17}$$

Or explicitly, for post-thermalization distances:

$$\langle C_k\rangle=\left[\int_0^\infty\sqrt{I}\mathcal{P}_I(I)\mathrm{d}I\right]^2\int_0^{2\pi}\cos(\theta_k)\mathcal{P}_\theta(\theta)\mathrm{d}\theta;\;\; k\geqslant 1 \tag{18}$$

with $\langle C_0\rangle$ as an exception:

$$\langle C_0\rangle=\int_0^\infty I\mathcal{P}_I(I)\mathrm{d}I=M_2=\langle\omega\rangle. \tag{19}$$

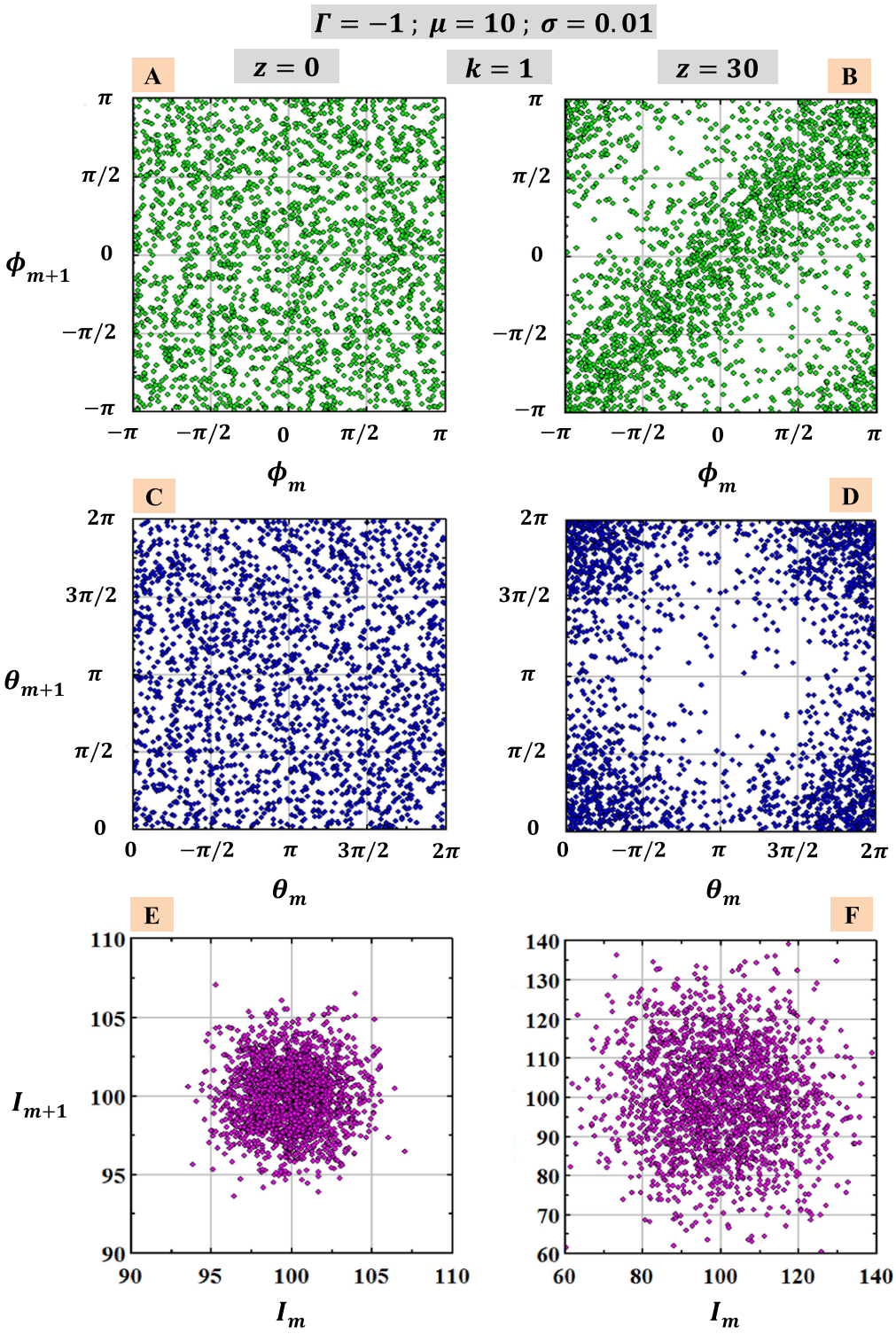

Figure 3. Nearest neighbors correlations. (A), (C), (E): $z = 0$. (B), (D), (F): $z = 30$. (A) and (B) Correlations of the field phases (ϕ). (B) Field phases are positively correlated (or negatively correlated for positive nonlinearity). The PDF of field phases ($\mathcal{P}_\phi(\phi)$) is flat on both (A) and (B) (the PDF is the set of integrals along vertical, or horizontal, slices). (C) and (D) Field phase differences (θ) are not correlated. (D) The PDF ($\mathcal{P}_\theta(\theta)$) is not flat anymore, having higher values near 0 and 2π (see figure 6). (E) and (F) Intensities are not correlated and their PDF ($\mathcal{P}_I(I)$) is of a Gaussian shape (much wider for $z = 30$, see figure 6). Uncorrelated intensities justify the quantum phase model approximation that led from equation (14) to (15).

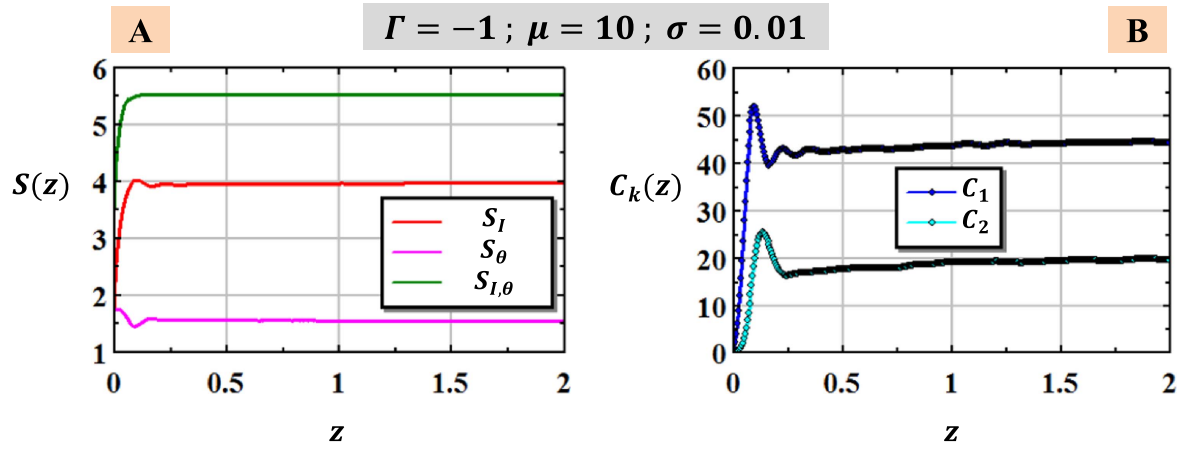

Figure 4. Evolution of entropies (A) and evolution of field correlations (B) simulated for a Gaussian-excited system. A: system entropy (green) is the sum of intensity-contributed entropy (red) and phase-difference (θ)-contributed entropy (magenta) ($s_{I,\theta} = s_I + s_\theta$). As the system evolves, under either focusing or defocusing nonlinearity, the field intensities spread, intensity-entropy shoots up showing even a small overshoot. Field phase differences on the other hand become correlated (see figure 3), the initially flat $\mathcal{P}_\theta(\theta)$ shrinks (see figure 5) and thus phase-difference-entropy goes down, even showing a small dip. Overall system's entropy ($s_{I,\theta}$) is monotonically increasing with evolution distance. B: field correlations are quickly formed, overshoot to a maximum value, degrade somewhat, and (unlike intensity correlations) continue to rise very slowly. Separation of entropies goes of course with two separated PDFs ($\mathcal{P}_I(I)$ and $\mathcal{P}_\theta(\theta)$, equation (16)).

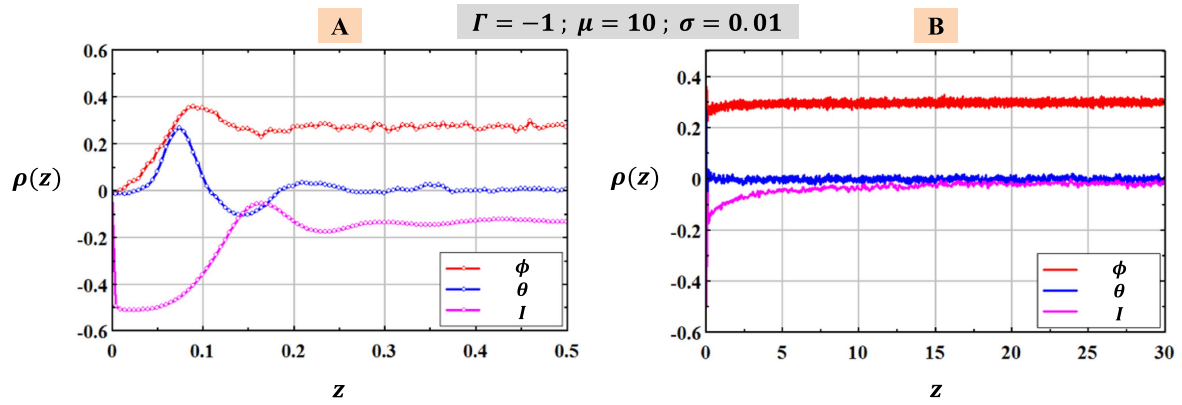

Figure 5. Evolution of nearest neighbors correlation coefficient—phases (red), phase differences (blue), and intensities (magenta). Early in the evolution, all three arrays show rather high degree of correlation (positive or negative) (A). However phase differences de-correlate very quickly (compared to the distance to thermodynamic equilibrium) and at $z = 0.2$ (for the simulated excitation parameters) phase-difference correlation coefficients are down to zero. Intensities strongly correlate (maximum correlation value and position of the maximum strongly depend on the initial amplitude spread), then quickly de-correlate to a certain value, and then gradually de-correlate further to a completely no correlation state (B). The only array (of the three presented) that stays correlated at long distances, positively correlated for negative (defocusing) nonlinearity and negatively correlated for positive (focusing) nonlinearity, is the array of phases. The level of the steady-state phase correlation depends on excitation parameters (particularly on the width of the exciting Gaussian).

Knowing $\mathcal{P}_I(I)$, the $\langle\sqrt{I}\rangle^2$ term of equation (17) can be calculated exactly. For $\sigma \ll \mu$ its value will turn out to be (to a very good approximation, *not* used in our calculations):

$$\langle\sqrt{I}\rangle^2 \cong M_1^2 \cong M_2; \ \ \sigma \ll \mu. \tag{20}$$

Regarding $\langle\cos(\theta_k)\rangle$, let us first treat the $k = 1$ case. For $k = 1$ we omit the subscript '1', i.e. $\theta_1 \equiv \theta$. For $\mathcal{P}_\theta(\theta)$ of equation (16) we then evaluate-

$$\langle\cos\theta\rangle = \frac{1}{2\pi\mathcal{I}_0(2\eta M_1^2)}\int_0^{2\pi}\cos\theta e^{-[2\eta M_1^2\cos\theta]}d\theta \tag{21}$$

and find:

$$\langle\cos\theta\rangle = (-1)\frac{\mathcal{I}_1(2\eta M_1^2)}{\mathcal{I}_0(2\eta M_1^2)}, \tag{22}$$

where $\mathcal{I}_n(z)$ is the modified Bessel function of the first kind.

Now to $\langle\cos(\theta_k)\rangle$ for $k \geqslant 2$. For $k = 2$ let us write

$$\theta_{m,2} = \theta_{m,1} + \theta_{m+1,1}. \tag{23}$$

It follows that

$$\langle\theta_2\rangle = \langle\theta_1 + \theta_1\rangle = \langle\theta_1\rangle\langle\theta_1|\theta_1\rangle \tag{24}$$

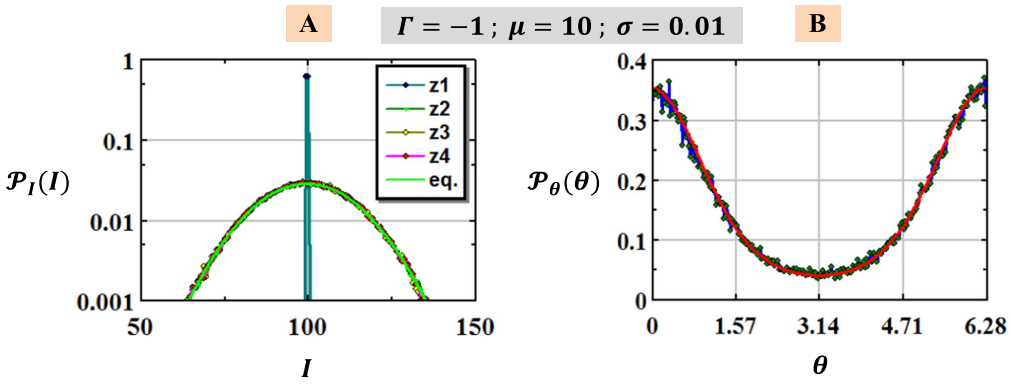

Figure 6. Probability density functions at thermodynamic equilibrium. (A) Simulated $\mathcal{P}_I(I)$ at $(z_1, z_2, z_3, z_4) = (0,\ 10,\ 20,\ 30)$ and an analytic curve (light green). (B) Simulated $\mathcal{P}_\theta(\theta)$ at $z = 30$ and an analytic curve (red). The simulated curves were averaged over 50 realizations. The continuous analytic curves were calculated according to equation (16).

And since θ_k are random variables (over realizations)

$$\langle\theta_2\rangle = \langle\theta_1\rangle^2 \equiv \langle\theta\rangle^2. \tag{25}$$

Similarly for $\langle\cos\theta_2\rangle$:

$$\langle\cos\theta_2\rangle = \langle\cos\theta\rangle^2 \tag{26}$$

From here the generalization is obvious:

$$\langle\cos\theta_k\rangle = \langle\cos\theta\rangle^k\,. \tag{27}$$

So equations (19) and (17) can be written as

$$\begin{aligned}\langle C_0\rangle &= \langle I\rangle = \langle\omega\rangle\\ \langle C_k\rangle &= \langle\sqrt{I}\rangle^2\langle\cos\theta\rangle^k\ ;\ k \geqslant 1.\end{aligned} \tag{28}$$

Equation (28) is general, and is not limited to Gaussian excitation. Equation (28) for field correlations in systems evolving under DNLSE dynamics holds for any long range fields distribution where the phase differences (θ_m's) are random (over realizations). The equation shows that if the phase differences are not flat-distributed (such that $\langle\cos(\theta)\rangle \neq 0$), the fields are correlated and exponentially decay. If $\langle\cos(\theta)\rangle$ is negative, the sign of the fields' correlations alternates with k.

With $\mathcal{P}_\theta(\theta)$ of equation (16) the correlations of equation (28) read:

$$\langle C_k\rangle = \langle\sqrt{I}\rangle^2\left[(-1)\frac{\mathcal{I}_1(2\eta M_1^2)}{\mathcal{I}_0(2\eta M_1^2)}\right]^k. \tag{29}$$

Or approximately:

$$\langle C_k\rangle \cong \langle\sqrt{I}\rangle^2\left[(-1)\left(\frac{x}{2} - \frac{x^3}{16} + \frac{x^5}{96}\right)\right]^k;\ x \equiv 2\eta M_1^2. \tag{30}$$

Equations (29) and (30) hold for both signs of the nonlinearity coefficient (Γ).

The PDFs ($\mathcal{P}_I(I)$, $\mathcal{P}_\theta(\theta)$) at thermodynamic equilibrium as well as the field correlations, depend on two parameters of the statistical excitation of fields' amplitudes—mean and width. For Gaussian excitation, we elected to replace the mean by the shift of amplitude distribution (μ) which, for $\sigma \ll \mu$ is very close to the mean. In the next five figures, we present thermodynamic-equilibrium properties of the system as a function of the two field amplitudes' excitation parameters (μ, σ). In all examples considered, fields phases at excitation ($z = 0$) are flat-distributed between 0 and 2π. For all simulations the number of sites in the periodic array is kept at $N = 2048$ and cyclic boundary conditions are assumed. All analytic curves are computed according to equations (16) and (29).

The curves of figure 7 were computed and simulated to show the effect of the sign of Γ (focusing or defocusing nonlinearity). Indeed both $\mathcal{P}_\theta(\theta)$ (figure 7(A)) and $\langle C_k\rangle$ (figure 7(B)) are affected by the sign of nonlinearity, as predicted by the corresponding equation (and as calculated for $\sigma = 0$ by [1]).

Next, figure 8(A) displays a map showing the normalized width (σ_I) of intensity PDF ($\mathcal{P}_I(I)$) at thermal equilibrium as a function of the two excitation parameters. The width (σ_I) of the thermalized intensities, as the map shows, depends on both parameters. Mathematically, as $\mathcal{P}_I(I)$ has a Gaussian shape, the normalized width (σ_I) is calculated through equation (16) to read:

$$\sigma_I = \frac{\sqrt{2\ln(\mathfrak{R}_I) + 1}}{\sqrt{|\eta\Gamma|}M_2}. \tag{31}$$

Back to figure 8(A), starting from the top-left corner of the map, spread of thermalized intensities is seen to increase with decreasing shift (μ) (i.e. decreasing nonlinearity) and with increasing excitation width (σ). Figure 8(B) shows a curve of the normalized intensity width (σ_I) versus excitation width (σ) for a fixed shift (μ). The insets just schematically illustrate the spread of excitation amplitudes.

The objective of figure 9 is to show 'universality' of $\mathcal{P}_\theta(\theta)$ in the sense of nonlinearity independence (above a certain threshold). Nonlinearity, just to restate, is proportional to M_2 that, for $\sigma \ll \mu$ is very close in its value to μ^2 (see equation (12)). The curves of figure 9(A) are simulated and calculated for $\mu = 4$, whereas the curves of figure 9(B) are for $\mu = 10$. Analytically, since the product ηM_1^2 is independent of μ, the curves of the two panels of figure 9 are identical. The simulated curves (averaged over 50 realizations) do show very small differences since the nonlinearity assumed for the left panel is not very high ($\mu^2 = 16$ on the left versus

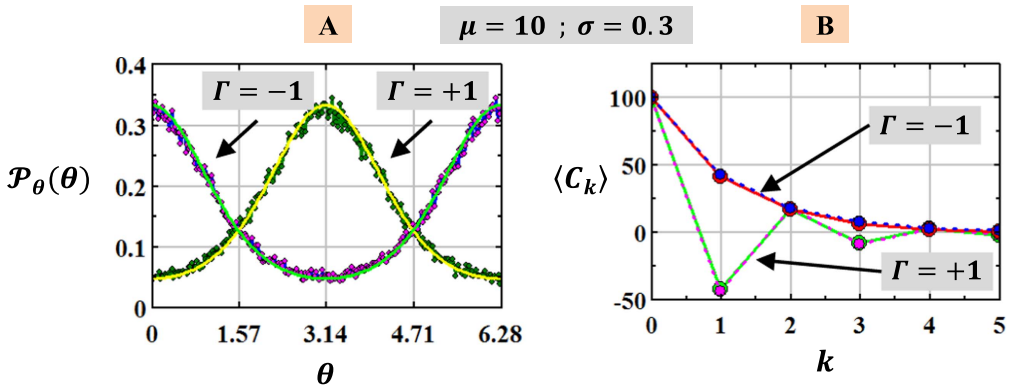

Figure 7. The effect of the nonlinearity sign on $\mathcal{P}_\theta(\theta)$ (A) and on $\langle C_k \rangle$ (B). The theoretical curves were calculated according to equations (16) and (29) respectively. (A) Continuous light-green and yellow curves are theoretical, green and magenta dots—simulations (averaged over 50 realizations). The $\mathcal{P}_\theta(\theta)$ curve is shifted by π upon change of the nonlinearity sign. (B) Red and light-green dots—theoretical, blue and magenta dots (and dashed lines in between to guide the eyes)—simulations (averaged over 50 realizations). The exponentially decaying correlations switch signs for odd site-distances (k) upon change of the nonlinearity sign. Note that according to equation (3) the field correlations are not normalized (in figure 11 we show normalized nearest neighbors field correlations).

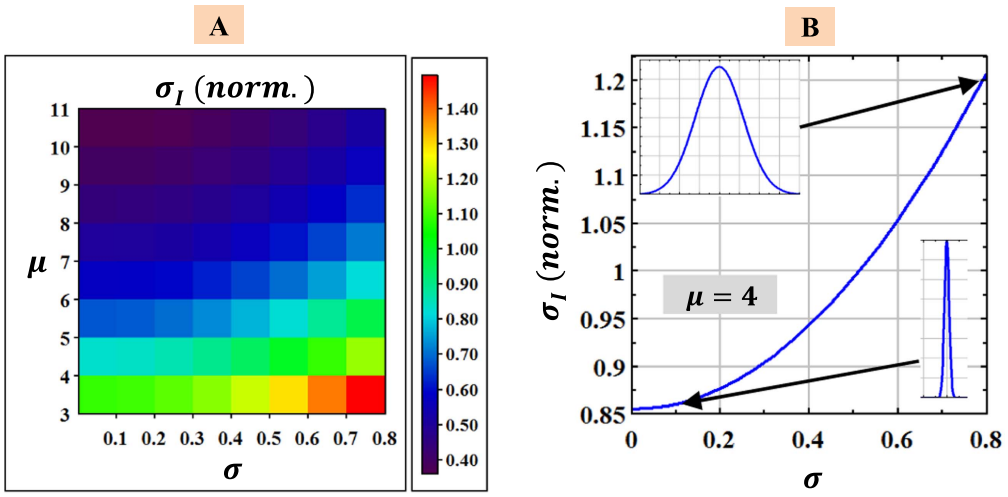

Figure 8. Normalized width σ of the PDF of thermalized field intensities ($\mathcal{P}_I(I)$) versus shift and width of the amplitude-exciting Gaussian. The normalized width (σ_I) of the PDF of site intensities at thermodynamic equilibrium is given by equation (31). The figure shows how strongly the field intensities spread with decreased nonlinearity and with increased width of Gaussian excitation (see figure 10(D)).

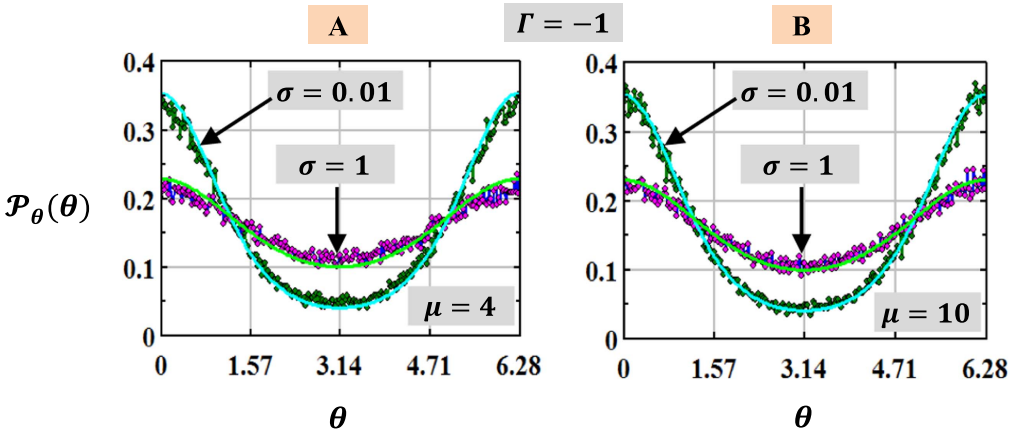

Figure 9. Universality of $\mathcal{P}_\theta(\theta)$ with respect to changes in the nonlinearity strength (that is proportional to $M_2 \cong \mu^2$). The analytic curves in (A) ($\mu = 4$) and (B) ($\mu = 10$) are identical and the simulated curves (averaged over 50 realizations) show rather small (A) versus (B) differences.

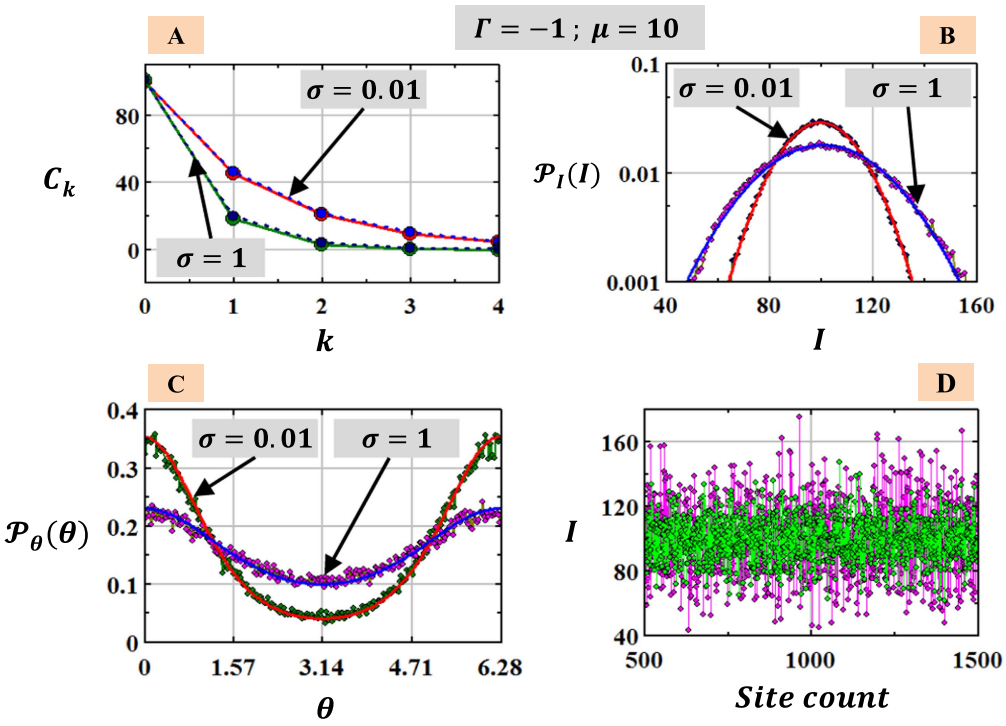

Figure 10. Effect of the spread of the excited field amplitudes (σ) on the post-thermalization characteristics of the fields. With increased width of excitation we see reduction in correlation strength and hence in shrinking of the correlation length (A), widening of the spread of field intensities ((B) and see figure 8), Flattening of the $\mathcal{P}_\theta(\theta)$ curve (C) and again, shown in a different manner, widening of the spread of field intensities (D, green for $\sigma = 0.01$ and purple for $\sigma = 1$).

$\mu^2 = 100$ on the right). It follows that correlation curves are also (nearly) universal in the same sense (nonlinearity independence, see figure 11).

The four panels of figure 10 show the effect of excitation width (σ) on system's characteristics at thermodynamic equilibrium (by both analytics and simulations). Each of the panels shows two curves, one for very small σ and one for a larger σ. For the larger σ, the four panels show lower correlations (A), wider $\mathcal{P}_I(I)$ distribution (B), flatter $\mathcal{P}_\theta(\theta)$ (C), and wider spread of field intensities (D). These shown effects do not come as a surprise since we have already seen (figure 2) that with increased σ the system moves upwards, i.e. towards higher temperatures, on the phase diagram.

The last figure, figure 11, is devoted to the universality of the correlation functions (the general equation (28) and the specific equation (29)). Again universality in the sense of the curves being virtually independent of the nonlinearity value ($\cong\mu^2$). The map and curve of figure 11 show only the (normalized) value of nearest neighbor fields' correlation (C_1/C_0), knowing that further away (C_k/C_0; $k > 1$) the correlations decay exponentially. Indeed the columns of the map are nearly mono-color (independent of μ). The very weak color change along the columns comes from the very weak dependence of the $\langle\sqrt{I}\rangle^2$ factor in the equations on the shift (since ηM_1^2 in the second factor (equation (29)) is independent of the shift (μ)).

Whereas the formed fields' correlations depend very weakly on nonlinearity, the color change going horizontally on the map of figure 11(A) and the single curve of figure 11(B) indicate how strongly the formed correlations depend on the width of the initially excited amplitudes. Wider spread of the excited amplitudes results in quick decay of the correlations' strength and thus a quick shrink of the correlation length.

6. Summary

We study a discrete optical system entertaining two effects—energy exchange between sites and on-site nonlinear interaction. The dynamics of the system is described by the DNLSE. Our study is focused on a special set of statistical excitations (values of the fields at $z = 0$). The amplitudes of the site-fields are excited with high mean and narrow width. The phases of the excited fields are random, flat-distributed around the full circle. Such excitations place the nonlinearity-dominated system in the thermalization zone of the phase diagram, at or slightly above the strong-interaction line ([27] and figure 2).

At thermodynamic equilibrium, the statistical characteristics of systems such-excited are analytically predictable. Systems' entropy is the sum of intensity-contributed entropy and phase-difference-contributed entropy ($s_{I,\theta} = s_I + s_\theta$). We have derived expressions, in terms of the moments of the statistical excitations, for the PDF of field intensities ($\mathcal{P}_I(I)$, equation (16)), for the PDF of field phase differences $\mathcal{P}_\theta(\theta)$, equation (16)), and for the formed field correlations ($\langle C_k\rangle$, equation (28)), all at thermodynamic equilibrium.

As the system evolves, very quickly strong field correlations are formed, overshooting, then decay slightly and

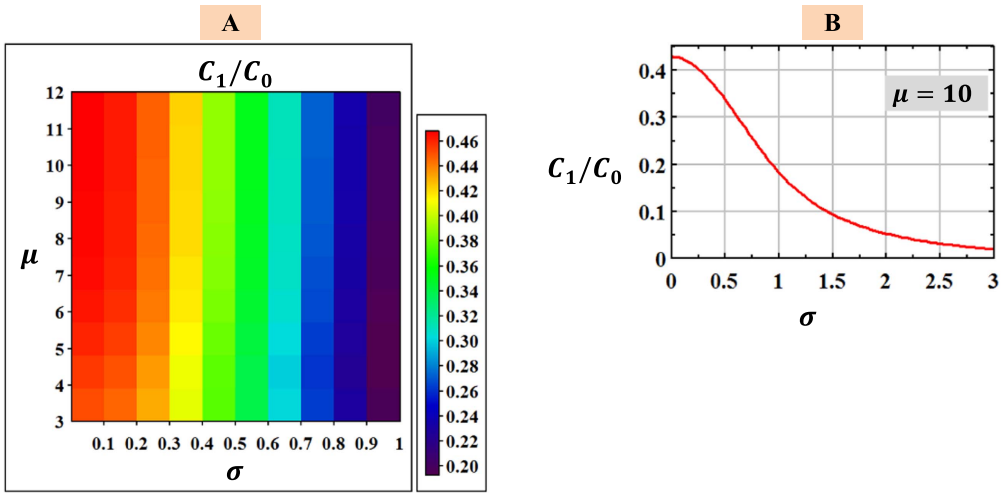

Figure 11. Dependence of the normalized nearest-neighbors correlation coefficient (C_1/C_0) on the excitation parameters (μ, σ) of the fields. The nearly mono-color columns of the map (A) indicate (near) universality in the correlation curves with respect to nonlinearity strength ($\cong\mu^2$). Going horizontally, the map (A) and the single curve (B) show strong decrease in correlation strength (and thus in correlation distance) with increased spread of the initially excited fields' amplitudes.

continue to slowly rise (or fall for odd neighbors count (k) and positive nonlinearity) towards their equilibrium value. At long distances field correlations decay exponentially with site-count (number of sites). The formed correlations are universal in the sense that correlation length very weakly depends on nonlinearity strength. However, the formed field correlations strongly shrink with increasing spread of the initially excited amplitudes.

Strong and negative second order (g_2), Hanbury Brown and Twiss type intensity correlations are quickly formed at the start of evolution (independent of the nonlinearity sign). But whereas formed first-order (g_1) field correlations persist to thermodynamic equilibrium, the formed intensity correlations gradually decay (see figure 5) due to constantly flowing wave-action ('density') currents.

Applying our derived expressions to Gaussian excitations, we find very good match of predicted and simulated steady-state system's characteristics.

The results of this study pertain not only to periodic 1D nonlinear optical waveguide arrays but generally to low or medium temperature 1D periodic systems evolving under DNLSE dynamics. For example, the formation of field correlations in the course of evolution (starting from zero at $t = 0$) was qualitatively stated by Polkovnikov *et al* [31] for a quench procedure applied to ultracold bosonic atoms trapped in an optical lattice.

Funding

This work was supported by DIP—German-Israeli Project Cooperation, by the BSF-NSF grant #2014719, by Icore—Israel Center of Research Excellence program of the ISF, and by the Crown Photonics Center. KY was supported by a scholarship from The Overseas Study Program of the China Scholarship Council.

ORCID iDs

Uri Levy https://orcid.org/0000-0002-6676-8990

References

[1] Silberberg Y, Lahini Y, Bromberg Y, Small E and Morandotti R 2009 Universal correlations in a nonlinear periodic 1D system *Phys. Rev. Lett.* **102** 233904
[2] Gati R and Oberthaler M K 2007 A bosonic Josephson junction *J. Phys. B: At. Mol. Opt. Phys.* **40** 10
[3] Kenkre V M and Campbell D K 1986 Self-trapping on a dimer: time-dependent solutions of a discrete nonlinear Schrödinger equation *Phys. Rev.* B **34** 4959
[4] Bustamante C A and Molina M I 1998 Selftrapping and quantum fluctuations in the discrete nonlinear Schrodinger equation arXiv:9809312
[5] Vardi A 2015 Chaos, ergodization, and thermalization with few-mode Bose–Einstein condensates *Rom. Rep. Phys.* **67** 67
[6] Miller P D, Scott A C, Carr J and Eilbeck J C 1991 Binding energies for discrete nonlinear Schrödinger equations *Phys. Scr.* **44** 6
[7] Bruinsma R, Maki K and Wheatley J 1986 Local modes in anharmonic solids and the Kondo problem *Phys. Rev. Lett.* **57** 14
[8] Fröhlich J and Park Y M 1978 Correlation inequalities and the thermodynamic limit for classical and quantum continuous systems *Commun. Math. Phys.* **59** 235–66
[9] Shirvanyants D, Panyukov S, Liao Q and Rubinstein M 2008 Long-range correlations in a polymer chain due to its connectivity *Macromolecules* **41** 1475–85
[10] Schwinger J 1951 On the Green's functions of quantized fields I *Proc. Natl Acad. Sci.* **37** 452–5
[11] Hadzibabic Z, Krüger P, Cheneau M, Battelier B and Dalibard J 2006 Berezinskii–Kosterlitz–Thouless crossover in a trapped atomic gas *Nature* **441** 1118–21
[12] Small E, Pugatch R and Silberberg Y 2011 Berezinskii–Kosterlitz–Thouless crossover in a photonic lattice *Phys. Rev.* A **83** 013806

[13] Galante M, Mazzarella G and Salasnich L 2014 Analytical results on quantum correlations of few bosons in a double-well trap arXiv:1410.5321
[14] Hennig D and Tsironis G P 1999 Wave transmission in nonlinear lattices *Phys. Rep.* **307** 333–432
[15] Kevrekidis P G 2009 *The Discrete Nonlinear Schrödinger Equation: Mathematical Analysis, Numerical Computations and Physical Perspectives* vol 232 (Berlin Heidelberg: Springer Science & Business Media) (https://doi.org/10.1007/978-3-540-89199-4)
[16] Ablowitz M J and Prinari B 2006 Nonlinear Schrödinger equations ed J P Françoise *et al Encyclopedia of Mathematical Physics* vol 5 (Amsterdam: Elsevier) p 552
[17] Eilbeck J C and Johansson M 2003 The discrete nonlinear Schrödinger *Proc. 3rd Conf.: Localization and Energy Transfer in Nonlinear Systems (June 17–21 2002 World Scientific) San Lorenzo de El Escorial, Madrid p 44 (arXiv: nlin/0211049)*
[18] Porter M A 2009 Experimental results related to discrete nonlinear Schrödinger equations arXiv:0907.4250
[19] Kartashov Y V, Malomed B A and Torner L 2011 Solitons in nonlinear lattices *Rev. Mod. Phys.* **83** 247
[20] Christodoulides D N and Joseph R I 1988 Discrete self-focusing in nonlinear arrays of coupled waveguides *Opt. Lett.* **13** 794–6
[21] Królikowski W and Kivshar Y S 1996 Soliton-based optical switching in waveguide arrays *JOSA* B **13** 876–87
[22] Aceves A B, De Angelis C, Peschel T, Muschall R, Lederer F, Trillo S and Wabnitz S 1996 Discrete self-trapping, soliton interactions, and beam steering in nonlinear waveguide arrays *Phys. Rev.* E **53** 1172
[23] Eisenberg H S, Silberberg Y, Morandotti R, Boyd A R and Aitchison J S 1998 Discrete spatial optical solitons in waveguide arrays *Phys. Rev. Lett.* **81** 3383
[24] Morandotti R, Peschel U, Aitchison J S, Eisenberg H S and Silberberg Y 1999 Dynamics of discrete solitons in optical waveguide arrays *Phys. Rev. Lett.* **83** 2726
[25] Christodoulides D N, Lederer F and Silberberg Y 2003 Discretizing light behaviour in linear and nonlinear waveguide lattices *Nature* **424** 817–23
[26] Droulias S, Lahini Y, Kominis Y, Papagiannis P, Bromberg Y, Hizanidis K and Silberberg Y 2013 Beam steering via peak power decay in nonlinear waveguide arrays *New J. Phys.* **15** 093038
[27] Rumpf B 2008 Transition behavior of the discrete nonlinear Schrödinger equation *Phys. Rev.* E **77** 036606
[28] Bagnato V S, Frantzeskakis D J, Kevrekidis P G, Malomed B A and Mihalache D 2015 Bose–Einstein condensation: Twenty years after arXiv:1502.06328
[29] Proukakis N P, Snoke D W and Littlewood P B (ed) 2017 *Universal Themes of Bose–Einstein Condensation* (Cambridge: Cambridge University Press)
[30] Dalfovo F, Giorgini S, Pitaevskii L P and Stringari S 1999 Theory of Bose–Einstein condensation in trapped gases *Rev. Mod. Phys.* **71** 463
[31] Polkovnikov A, Sachdev S and Girvin S M 2002 Nonequilibrium Gross–Pitaevskii dynamics of boson lattice models *Phys. Rev.* A **66** 053607
[32] Pelinovsky D E 2011 *Localization in Periodic Potentials: From Schrödinger Operators to the Gross–Pitaevskii Equation* vol 390 (Cambridge: Cambridge University Press)
[33] Endres M 2014 Probing correlated quantum many-body systems at the single-particle level *PhD Thesis* Ludwig Maximilians University, München, Germany
[34] Danshita I and Polkovnikov A 2011 Superfluid-to-Mott-insulator transition in the one-dimensional Bose–Hubbard model for arbitrary integer filling factors *Phys. Rev.* A **84** 063637
[35] Greiner M, Mandel O, Esslinger T, Hänsch T W and Bloch I 2002 Quantum phase transition from a superfluid to a Mott insulator in a gas of ultracold atoms *Nature* **415** 39–44
[36] Bloch I 2005 Ultracold quantum gases in optical lattices *Nat. Phys.* **1** 23–30
[37] Kollath C, Läuchli A M and Altman E 2007 Quench dynamics and nonequilibrium phase diagram of the Bose–Hubbard model *Phys. Rev. Lett.* **98** 180601
[38] Choi J Y, Hild S, Zeiher J, Schauß P, Rubio-Abadal A, Yefsah T, Khemani V, Huse D A, Bloch I and Gross C 2016 Exploring the many-body localization transition in two dimensions *Science* **352** 1547–52
[39] Johnsson M T, Dennis G R and Hope J J 2013 Squeezing in Bose–Einstein condensates with large numbers of atoms *New J. Phys.* **15** 123024
[40] Altman E 2015 Non equilibrium quantum dynamics in ultra-cold quantum gases arXiv:1512.00870
[41] Chatterjee S and Kirkpatrick K 2012 Probabilistic methods for discrete nonlinear Schrödinger equations *Commun. Pure Appl. Math.* **65** 727–57
[42] Makris K G, Musslimani Z H, Christodoulides D N and Rotter S 2015 Constant-intensity waves and their modulation instability in non-Hermitian potentials *Nat. Commun.* **6** 7257
[43] Rasmussen K Ø, Cretegny T, Kevrekidis P G and Grønbech-Jensen N 2000 Statistical mechanics of a discrete nonlinear system *Phys. Rev. Lett.* **84** 3740
[44] Garanovich I L, Longhi S, Sukhorukov A A and Kivshar Y S 2012 Light propagation and localization in modulated photonic lattices and waveguides *Phys. Rep.* **518** 1–79
[45] Mandelik D, Eisenberg H S, Silberberg Y, Morandotti R and Aitchison J S 2003 Band-gap structure of waveguide arrays and excitation of Floquet-Bloch solitons *Phys. Rev. Lett.* **90** 053902
[46] Yariv A 1991 *Optical Electronics* (Philadelphia, PA: Saunders) ch 13
[47] Haus H, Huang W, Kawakami S and Whitaker N 1987 Coupled-mode theory of optical waveguides *J. Lightwave Tech.* **5** 16–23
[48] Smerzi A, Fantoni S, Giovanazzi S and Shenoy S R 1997 Quantum coherent atomic tunneling between two trapped Bose–Einstein condensates *Phys. Rev. Lett.* **79** 4950
[49] Lieb E H, Seiringer R, Solovej J P and Yngvason J 2005 *The Mathematics of the Bose Gas and its Condensation* vol 34 (Basel-Boston-Berlin: Birkhäuser Verlag) (https://arxiv.org/pdf/cond-mat/0610117.pdf)
[50] Scott A C and Macneil L 1983 Binding energy versus nonlinearity for a 'small' stationary soliton *Phys. Lett.* A **98** 87–8
[51] Yukalov V I and Yukalova E P 2015 Statistical models of nonequilibrium Bose gases arXiv:1502.06244
[52] Chin C, Grimm R, Julienne P and Tiesinga E 2010 Feshbach resonances in ultracold gases *Rev. Mod. Phys.* **82** 1225
[53] Fedichev P O, Reynolds M W and Shlyapnikov G V 1996 Three-body recombination of ultracold atoms to a weakly bound s level *Phys. Rev. Lett.* **77** 2921
[54] Liu C S, Yin Z Z, Wu Y D, Xu T F, Wen L H and Chen S 2016 Topologically nontrivial states in one-dimensional nonlinear bichromatic superlattices arXiv:1603.06296
[55] Levy U and Silberberg Y 2014 Electrical-field distributions in waveguide arrays—exact and approximate arXiv:1401.0642
[56] Seaman B T, Carr L D and Holland M J 2005 Nonlinear band structure in Bose–Einstein condensates: nonlinear Schrödinger equation with a Kronig–Penney potential *Phys. Rev.* A **71** 033622
[57] Rebuzzini L, Artuso R, Fishman S and Guarneri I 2007 Effects of atomic interactions on quantum accelerator modes *Phys. Rev.* A **76** 031603
[58] Burger S, Bongs K, Dettmer S, Ertmer W, Sengstock K, Sanpera A, Shlyapnikov G V and Lewenstein M 1999 Dark

solitons in Bose–Einstein condensates *Phys. Rev. Lett.* **83** 5198

[59] Perrin A, Bücker R, Manz S, Betz T, Koller C, Plisson T, Schumm T and Schmiedmayer J 2012 Hanbury Brown and Twiss correlations across the Bose–Einstein condensation threshold *Nat. Phys.* **8** 195–8

[60] Bishop A R, Jiménez S and Vázquez L (ed) 1995 *Fluctuation Phenomena: Disorder and Nonlinearity* (Singapore: World Scientific)

[61] Finlayson N and Blow K J 1994 Hamiltonian chaos in the Discrete nonlinear Schrödinger equation *Chaos Solitons & Fractals* **4** 1817–34

[62] Sarma A K, Miri M A, Musslimani Z H and Christodoulides D N 2014 Continuous and discrete Schrödinger systems with parity-time-symmetric nonlinearities *Phys. Rev.* E **89** 052918

[63] Korabel N and Zaslavsky G M 2007 Transition to chaos in discrete nonlinear Schrödinger equation with long-range interaction *Phys. A: Stat. Mech. Appl.* **378** 223–37

[64] Polkovnikov A, Altman E, Demler E, Halperin B and Lukin M D 2005 Decay of superfluid currents in a moving system of strongly interacting bosons *Phys. Rev.* A **71** 063613

[65] Huber S D, Theiler B, Altman E and Blatter G 2008 Amplitude mode in the quantum phase model *Phys. Rev. Lett.* **100** 050404

[66] Singer K (ed) 2007 *Statistical Mechanics* vol 2 (London: Royal Society of Chemistry) (https://doi.org/10.1039/9781847556936)

[67] Santra B, Baals C, Labouvie R, Bhattacherjee A B, Pelster A and Ott H 2017 Measuring finite-range phase coherence in an optical lattice using Talbot interferometry *Nat. Commun.* **8** 15601